We are IntechOpen, the world's leading publisher of Open Access books Built by scientists, for scientists

4,800
Open access books available

122,000
International authors and editors

135M
Downloads

Our authors are among the

154
Countries delivered to

TOP 1%
most cited scientists

12.2%
Contributors from top 500 universities

CLARIVATE ANALYTICS BOOK CITATION INDEX INDEXED

WEB OF SCIENCE™

Selection of our books indexed in the Book Citation Index in Web of Science™ Core Collection (BKCI)

Interested in publishing with us?
Contact book.department@intechopen.com

Numbers displayed above are based on latest data collected.
For more information visit www.intechopen.com

4

Progress in Continuous-Wave Supercontinuum Generation

Arnaud Mussot and Alexandre Kudlinski
Laboratoire PhLAM, IRCICA, Université Lille 1
France

1. Introduction

Supercontinuum (SC) light sources are nowadays a very common way to access a large span of wavelengths, usually ranging from the near ultraviolet (around 400 nm) to the infrared (around 2.4 μm). It corresponds to a range of interest for many applications in optics for measuring transmission, dispersion, or in biophotonics for achieving fluorescence microscopy, optical coherence tomography... Indeed these sources are really promising because they should allow to replace the N laser sources used in these experimental setups to access to all theses wavelengths by a single broad one and a spectral filtering apparatus. Most of these results have been obtained by using powerful pump lasers of several kilo-Watts peak power, operating from the femtosecond (Titane:Saphire) to the nanosecond regimes (Nd:YAG), launched in the low dispersion region of a microstructured optical fiber. Although these fibers are short enough (typically from 1 to 10 m) to neglect the linear absorption during the propagation of the pump, the spectral power density is relatively low (few hundreds of μw/nm) which could limit the implementation of SC sources in many application devices. This is related to a technological limitation of the pump source because it is not easy to combine strong peak power and high average power. One of the simplest solutions to increase the the spectral power density of SC sources is to replace pulsed sources with continuous-wave (CW) light sources whose available average powers are much more important. We will see that the dynamics of SC formation is considerably different in this case, requiring to perform intensive numerical studies to optimize the fiber parameters. Indeed, longer fibers are required (from tens to hundreds of meters) which heightens sensitivity to fiber attenuation, namely of the OH pic absorption, that strongly impacts the soliton evolution. However extremely powerful SCs have been reported with more than 10 mW/nm of spectral power density. Furthermore, these pump sources are usually all-fiber that leads to a second advantage against most of pulsed SC because CW pump can be directly spliced on the PCF. It is also important to point out that these SC sources have different temporal properties than the ones of pulsed SCs.

The first experimental demonstration of CW SC have been realized at the end of the nineties with a Raman laser launched in a standard telecommunication fiber. The spectral broadening was relatively restricted (around 200 nm) because it was mainly due to Raman effect Gonzalez-Herraez et al. (2003); Persephonis et al. (1996); Prabhu et al. (2000). A breakthrough was reached a few years later when stronger pump lasers (from more than one order of magnitude) based on Ytterbium doped fibers were combined with photonic crystal fibers

(PCFs) owing a low group-velocity dispersion (GVD) value around the pump wavelength Avdokhin et al. (2003). With these setups, SC generation was mainly due to solitonic effects like in pulsed SC. A renew of interest for these sources started from 2007 where first numerical demonstrations of very broad CW SC were reportedMussot et al. (2007), just followed by experimental demonstrationsCumberland et al. (2008a); Kudlinski & Mussot (2008).
As an example, a typical and simple experimental setup used for SC generation is schematized in Fig. 1. In our experimental configuration used for the experiments hereafter, the PCFs were

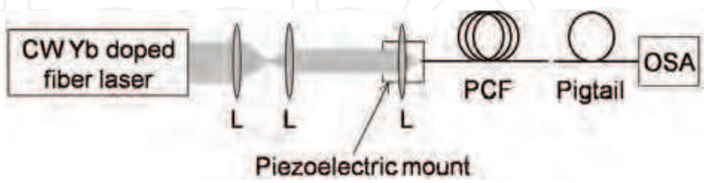

Fig. 1. Scheme of the experimental setup used for the SC generation experiments. L : lens.

pumped with ytterbium-doped fiber laser delivering either 20 W at 1064 nm with a full width at half maximum of 0.5 nm, or 50 W or 100 W at 1070 nm with a full width at half maximum of 1 nm. The output beam diameter of the laser was reduced with an afocal setup and the beam was then launched into the fiber with appropriate aspheric lenses (of a few mm focal length). All lenses were antireflection coated and a heat dissipater was carefully placed on top of the V-groove supporting the PCF in order to manage thermal issues caused by the high power laser. This allowed to greatly improve the temporal stability of the injection setup and no noticeable change in coupling efficiency was observed for several tens of minutes at full pump power. The coupling efficiency in these conditions was typically 70%–80%. The output of the fiber was butt-coupled to a pigtail to reduce the power launched inside the optical spectrum analyzer (OSA). All-fiber schemes are also used Cumberland et al. (2008a) but splicing issues are usually more -time-consuming for a lab experiment than free-space coupling.

2. Basic mechanisms of continuous-wave supercontinuum generation

Mechanisms at the origin of SC are now well knownCumberland et al. (2008b); Dudley et al. (2006); Kobtsev & Smirnov (2005); Mussot et al. (2007); Travers et al. (2008); Vanholsbeeck et al. (2005). The modulationnal instability (MI) process is at the origin of the formation of CW SC. It originates from the perfect balance between linear and nonlinear effects experienced by a strong field, the pump, and a small perturbation, the noise, when working in anomalous GVD region of an optical fiber. At the beginning of the fiber, this small perturbation is amplified. The typical signature of this process in the spectral domain is two symmetric side lobes located around the pump (Figs. 2-(a) and (b)). By further propagating into the fiber, this small periodic perturbation is amplified to become a train of solitonic pulses (Figs. 2-(c)and (d)). Note that these pulses have not identical characteristics as they originate from a process that is seeded by noise. On the other hand, we remind that in the case of a single soliton propagating in an optical fiber, it is well known that during its propagation, it is disturbed by higher order dispersion orders effect and as a consequence it shed energy to radiations called dispersive waves (DWs) which verify a phase matching condition. This leads to the generation of DWs on the short wavelength side of the soliton and to a red shift of the soliton, called *spectral recoil* for momentum conservation (Figs. 3-(a) and (b)). The consequence of the phase matching condition, is that solitons and DWs do not travel at the same velocity. If no additional effect is experienced by these waves, they will no longer interact again during their respective

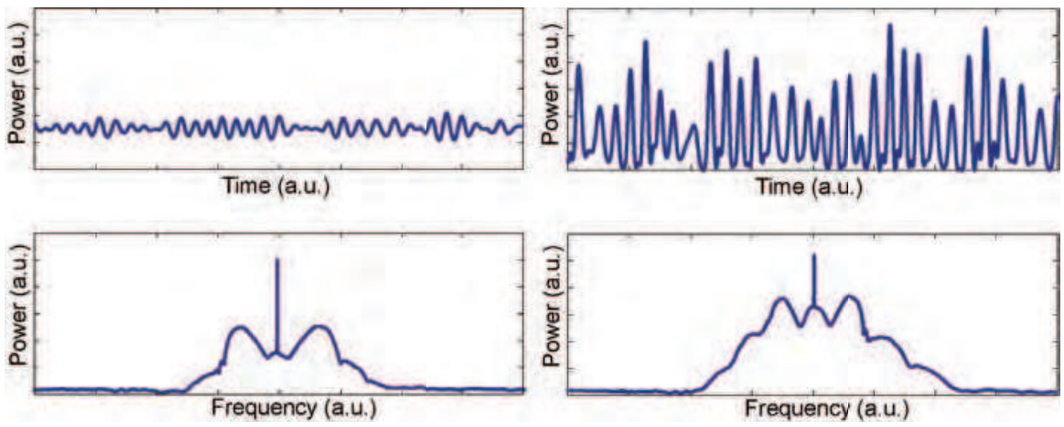

Fig. 2. Schemes illustrating the first steps of modulationnal instability, (a)-(b) at the beginning of the process when the small perturbation starts to grow and (c)-(d) when the solitonic train is created. (a) and (c) correspond to the time domain, and (b) and (d) correspond to the frequency domain.

propagation. However, during the propagation of solitons, because they are strong waves, the Raman effect induces an additional and continuous red shift of their central frequencies . This effect is called soliton self-frequency shift (SSFS)Gordon (1986) and decelerates the soliton because the group index increases with frequency in usual fibers (Fig. 3-(c)). As a consequence, as the velocity of DWs has not changed, the solitons can interact again with them via the cross-phase modulation effectGenty et al. (2004) which shifts DWs toward short wavelengths. Finally, it is important to understand that this group velocity matching is the rule that allows to connect lower and upper limits of SCs (Figs. 3-(d))Stone & Knight (2008). This is different in fibers with two zero dispersion wavelengths (ZDWs). When the soliton approaches the second ZDW, it still generates DWs but on the long wavelength side of the SCGenty et al. (2004); Mussot et al. (2007). The spectral recoil tends now to shift it on the opposite side that the one of the SSFS. An equilibrium is reached and the frequency shift of the soliton is cancelledSkryabin et al. (2003). In this case solitons and DWs will no interact together and no trapping mechanism will occur like it is the case in fiber with a single ZDW.

3. Bandwidth-limited near infrared continuous-wave supercontinuum

The interest of limiting the spectral extension of CW SC is to concentrate of the available power in the desired spectral span. This is achieved in fibers with two ZDWs in which the SSFS can be cancelled by the spectral recoil effect experienced by solitons located just below the second zero dispersion wavelength. By this way, increasing the power leads to an increase of the power spectral density.

3.1 Double zero-dispersion wavelength photonic crystal fibers

It is possible to design PCFs with two ZDWs from part to part of the pump wavelength at 1064 nm, and a low anomalous dispersion region at this wavelength. Such group-velocity dispersion (GVD) curves can be achieved with a relatively small hole-to-hole spacing Λ in the order of 1.7 μm and a d/Λ value in the range of 0.4–0.5 (d is the hole diameter) Mussot et al. (2007); Tse et al. (2006). It is well known that a microstructured cladding with these geometrical properties would lead to relatively high confinement losses at wavelengths around 1.5 μm which is the reason why 10 periods of holes were necessary between the core

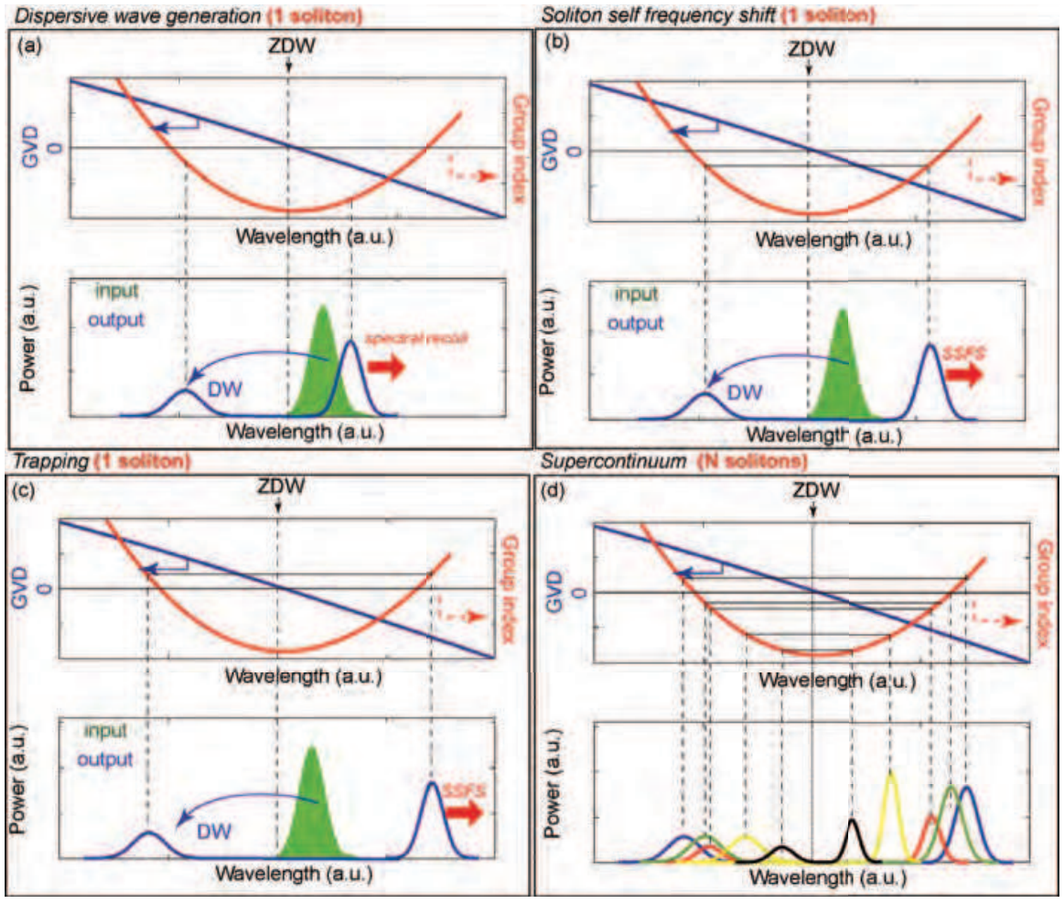

Fig. 3. Schemes illustrating (a) the DW generation from a single soliton, (b) the SSFS effect and (c) the trapping of teh DW by the soliton, *for a single soliton*. In each cases, the dispersion curve is represented in blue and the group index curve in red. (d) Schemes illustrating the formation of a CW SC, *involving N solitons*.

and the external jacket to decrease confinement losses to an acceptable values of a few dB/km at 1550 nm, at which the SC is expected to be generated. Figure 4(a) displays a scanning electron microscope (SEM) image of such a PCF (labelled fiber C in what follows, see Table 1). Another important issue in CW SC generation is the absorption of the water band centered at 1380 nm Cumberland et al. (2008a). We thus performed a chemical cleaning of the stacked preform under halogenic atmosphere to reduce surface contamination and to lower the water content. This allowed to decrease the peak attenuation at 1380 nm from typically 600 dB/km (without any special treatment) to about 120 dB/km. A typical attenuation spectrum is shown in Fig. 4(b) for fiber C, which SEM is represented in Fig. 4(a). The background loss being around 30 dB/km at 1380 nm, the contribution of the water contamination is about 90 dB/km at 1380 nm.

Three different PCF samples (labeled A, B and C) are investigated here. These fibers are characterized by slightly differing Λ and d/Λ values so that the GVD curve of each fiber is slightly different. The GVD curves are represented in Fig. 5(a), where the vertical line represents the pump wavelength. All GVD curves have been calculated with a finite-elements

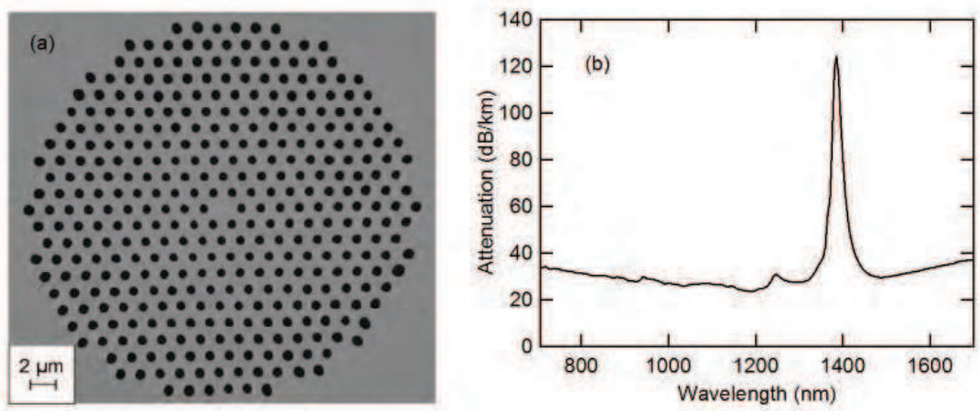

Fig. 4. (a) Typical SEM image of PCFs used for infrared CW supercontinuum. (b) Typical attenuation spectrum.

Parameter	Fiber A	Fiber B	Fiber C
ZDW1 (nm)	1012	958	903
ZDW2 (nm)	1236	1346	1570
γ at 1064 nm ($W^{-1}.km^{-1}$)	22	24	30
GVD at 1064 nm (ps/nm/km)	+4	+12	+30

Table 1. Parameters of the PCFs under investigation in this section.

method (FEM) from high resolution SEM images of the PCFs. Table 1 summarizes the properties of the three fibers under investigation.

3.2 Control of the supercontinuum long-wavelength edge

The experiments reported in this section were performed in 100 m-long samples of each PCF described in Table 1. In the launching conditions described in the previous paragraph, the output power were respectively 7.35 W, 7.25 W and 7.16 W for fibers A to C, with a 20 W CW fiber laser at 1064 nm. Figure 5(b) shows the spectra obtained in all fibers. The green curve corresponds to fiber A, with the closest ZDWs. As expected from Ref. Mussot et al. (2007), the spectral width is limited by the second ZDW. The dispersion value at the 1064 nm pump wavelength is very low (+4 ps/nm/km). The spectral broadening is thus initially dominated by MI, with the anti-Stokes MI sideband overlapping with the normal GVD region. The short wavelength extension just below the first ZDW results from a spectral overlap of MI sidebands and blue-shifted dispersive wave in the normal GVD region, as analyzed in Cumberland et al. (2008b). Since the spectral position of the Stokes MI sidebands is just below the second ZDW of the fiber, the SSFS is very short and the spectrum remains consequently quite symmetric. The power generated above the second ZDW (depicted by a vertical line) is attributed to the generation of red-shifted dispersive waves accompanying the cancelation of the SSFS. The red curve in Fig. 5(b) corresponds to the spectrum measured for fiber B, with both ZDWs separated by about 400 nm. In this fiber, the long-wavelength ZDW is very close to the center of the water absorption band (1380 nm). It is well known that the SSFS is canceled if a second ZDW is present at longer wavelengths Skryabin et al. (2003), which is the case here. This is seen in the red spectrum of Fig. 5(b) as a peak centered at 1310 nm, which corresponds

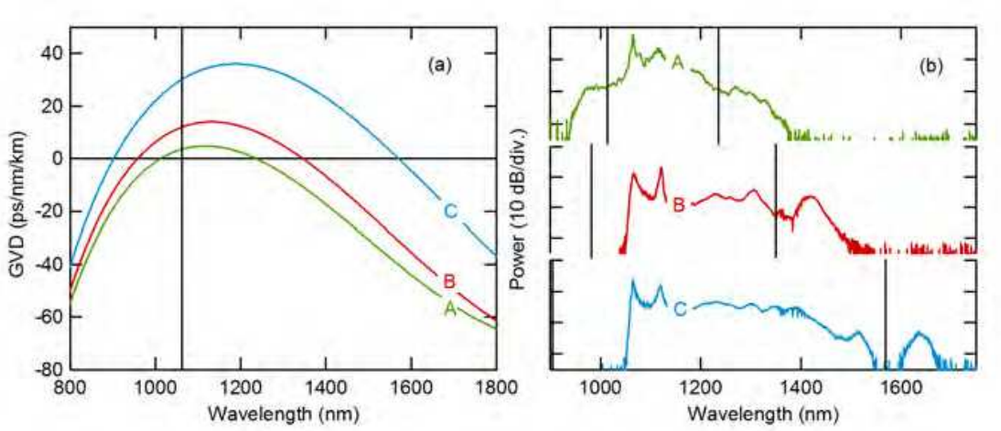

Fig. 5. (a) GVD curves of the three PCFs under investigation in this section. The vertical line depicts the pump wavelength. (b) Corresponding output spectra recorded for a fiber length of 100 m and a pump power of 12.5 W launched into the PCFs. Vertical lines represent the ZDWs.

to an accumulation of all solitons stopped by the second ZDW. Additionally, a large part of energy is transferred to a dispersive wave centered at 1420 nm, which is phase-matched with the solitons. In fiber C displayed in Fig. 5(b) in blue, the flatness of the spectrum is clearly affected by the water absorption at 1380 nm. This can be seen as a spectral decrease at wavelengths higher than 1380 nm. The higher energy solitons are able to tunnel through the water attenuation band and are then stopped by the second ZDW located at 1570 nm in fiber C. The less energetic ones stop just below 1380 nm due to the water absorption peak. As in fiber B, an accumulation of solitons is seen just before the second ZDW, and a dispersive wave which is phase-matched with the solitons is generated at 1630 nm. Note that the peak located around 1120 nm is due to Raman lasing because of Fresnel reflection at both fiber faces. It is also important to note that, unlike in fiber A, no short wavelength extension is observed in fibers B and C. Indeed, in these fibers, the amount of energy transferred from solitons to blue-shifted dispersive waves is negligible because there is no spectral overlap between solitons and dispersive waves Akhmediev & Karlsson (1995).

3.3 Dynamics of the supercontinuum formation

To go further into the detailed dynamics of SC formation, we performed a cut-back measurement on fiber C. The spectrum was measured every 5 m for fiber lengths between 0.5 and 100 m. The results are displayed in Fig. 6, where the output spectra are represented as a function of fiber length. The solitonic waves created by MI are progressively red-shifted by SSFS during the first 30 m of propagation. They are then stopped by the second ZDW located at 1570 nm (depicted by the white dotted vertical line). The soliton build-up due to spectral recoil before the second ZDW can be seen as an increase in spectral power. The red-shifted dispersive wave is also observed from this propagation length of 30 m. For more important fiber lengths, the spectrum extension remain almost constant. The experimental results displayed in Figs. 5 and 6 illustrate the possibility of tailoring the spectrum extent in the context of multi-watt and relatively flat SC generation. The long-wavelength edge of the spectrum is limited by red-shifted dispersive waves, whose spectral location is imposed by the second ZDW.

4. Extension towards visible wavelengths

Another long term issue of CW-pumped SC concerns the lack of short wavelengths generation when pumping at 1 μm. The generation of visible wavelengths would be of great interest for a substantial number of applications including high resolution imaging, metrology or spectroscopy. One possible approach to achieve this is to take advantage of the process of dispersive wave trapping by solitons Nishizawa & Goto (2002). This process leads to an extra blue shift of dispersive waves in the spectral domain Genty et al. (2004; 2005); Gorbach & Skryabin (2007a;b); Gorbach et al. (2006); Travers (2009); Travers & Taylor (2009). Experimentally, this phenomenon has been proved to be of primary importance to generate short wavelengths in pulsed pumping regime Stone & Knight (2008). It has also been combined with dispersion-engineered PCFs to further extend SC to the UV in nanosecond and picosecond pumping schemes Kudlinski et al. (2006). This idea consists in modifying the dispersion curve along the fiber so that group-velocity matching conditions for trapped dispersive waves continuously evolve along propagation. This leads to the generation of new wavelengths as the ZDW decreases along propagation. The present work is based on this idea which has been adapted to CW pumping conditions.

4.1 Zero-dispersion wavelength decreasing photonic crystal fibers

The dispersion-engineered PCF firstly used within this framework consists of a 100 m-long section with a constant dispersion followed by a 100 m-long section with decreasing ZDW, as illustrated in Fig.7(c). The total attenuation of the 200 m-long PCF is 1.5 dB at 1064 nm. A SEM image of the input and output faces of the PCF is represented in Figs. 7(a) and (b) respectively, with the same scale. The input outer diameter is 125 μm, the hole-to-hole spacing Λ is 4.7 μm and the hole diameter d is 2.6 μm. The dispersion curves at the PCF input and output have been computed with a finite elements method from high resolution SEMs and are represented

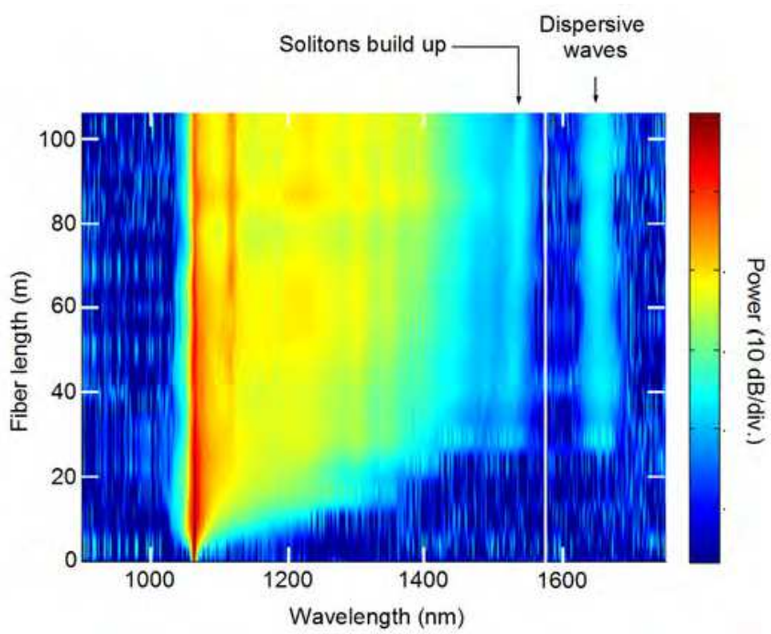

Fig. 6. Experimental measurement of the SC dynamics as a function of fiber length, in fiber C. The white vertical line represent the second ZDW.

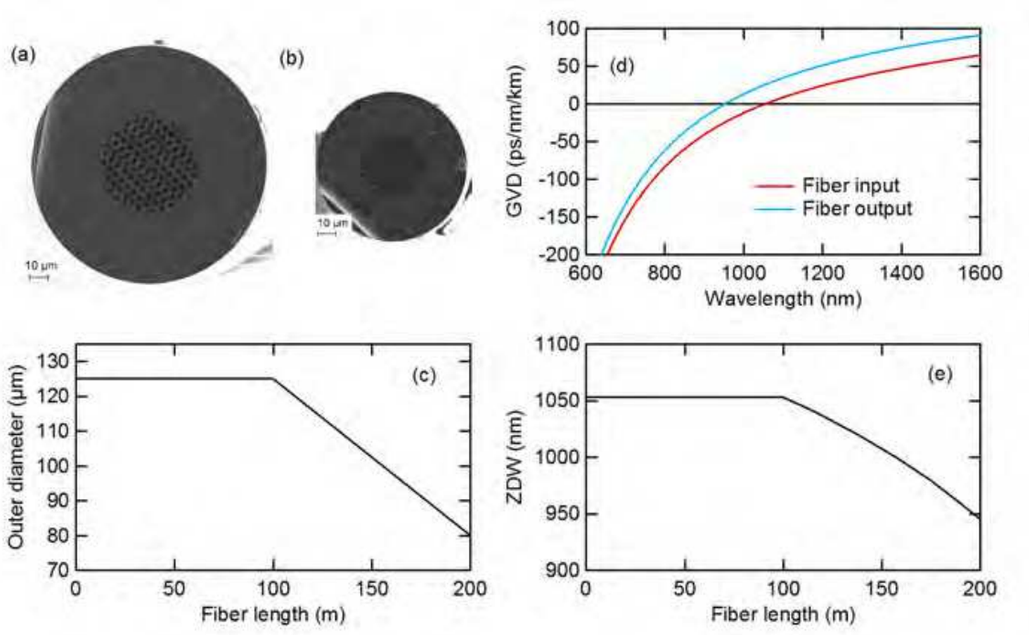

Fig. 7. (a),(b) SEMs of the input and output faces of the ZDW decreasing fiber. Respective outer diameters are 125 and 80 μm. (c) Outer diameter versus fiber length. (d) GVD curves at the input (red line) and output (blue line) of the ZDW decreasing fiber. (e) ZDW versus fiber length.

in Fig. 7(d) in red and blue lines, respectively. The input ZDW is located at 1053 nm, just below the pump wavelength of 1064 nm. To decrease the size of the microstructure along propagation and consequently shift the ZDW toward shorter wavelengths, the outer diameter of the fiber has been approximately linearly reduced to a final diameter of 80 μm (see Fig. 7(c)). This was done by gradually increasing the drawing speed during the fiber fabrication whilst keeping the preform feed rate constant. The pitch Λ at the fiber output was reduced to 3.1 μm and the d/Λ ratio was kept constant along the whole PCF, so that the output ZDW is shifted down to 950 nm. The longitudinal evolution of the ZDW of the PCF is represented in Fig. 7(e). In the first 100 m, the ZDW is fixed to 1053 nm, and it drops to 950 nm in a quasi-linear way along the last 100 m.

4.2 Generation of visible light

The setup used to pump the fabricated PCF is shown in Fig. 1. The beam from a 20 W CW fiber laser at 1064 nm was collimated and launched into the fiber with a lens of 4.5 mm focal length. The coupling efficiency was 75%, corresponding to a power of 13.5 W launched into the PCFs.

The SC spectrum measured at full pump power in the ZDW-decreasing PCF described above displayed in Fig. 8 in red line. It is ranging from 670 nm to 1350 nm with an output power of 9.5 W. Additional spectral components are located around 550 nm and the visible part of the SC was easily observable with naked eye at the PCFs output. The inset of Fig 8 displays a far-field image of the whole visible spot observable at the PCF output. Since the modal distribution of the SC does not look single mode, the far-field profile was investigated as a function of wavelength by using 10 nm bandpass filters. Right insets of Fig. 8 show far-field

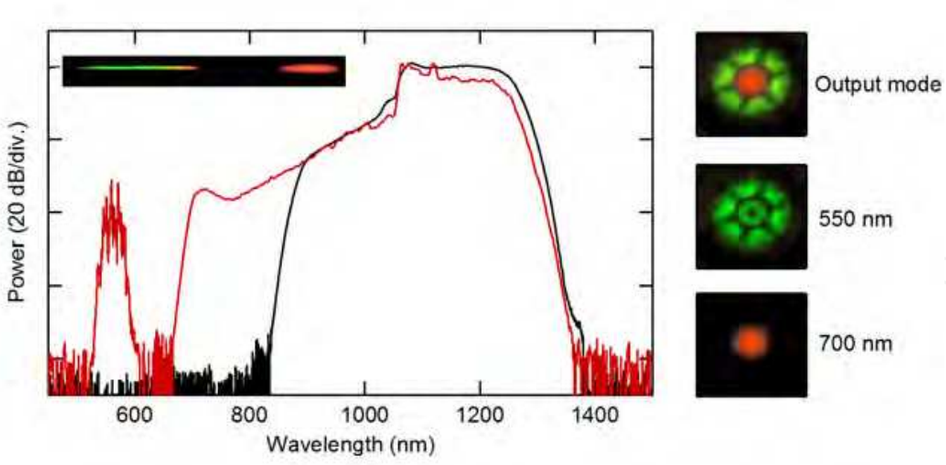

Fig. 8. Output spectra obtained in the uniform PCF (black line) and in the ZDW-decreasing one (red line). Inset: output beam dispersed by a prism. Right: output far-field without any filter (top), with a 550 nm filter (center) and with a 700 nm filter (bottom).

images centered at 550 nm and 700 nm . The green spectral components located around 550 nm are clearly generated in higher-order modes. This part of the spectrum was not expected from our design and is probably due to a phase-matching condition satisfied with higher-order modes Efimov et al. (2003); Omenetto et al. (2001). The far-field image recorded at 700 nm shows that the red spectral components are generated in a fundamental mode. We also checked that the mode was fundamental-like in the whole spectrum above 700 nm for all fibers.

A uniform PCF with dispersion comparable to the ZDW-decreasing fiber input was used for comparison. The output spectrum obtained in the same conditions than above is displayed in Fig. 8, in grey line. It extends up to 1355 nm into the infrared, which is very similar to the spectrum obtained in the ZDW-decreasing PCF. However, the short-wavelength edge is located at about 840 nm, which is much less spectacular than in in the ZDW-decreasing PCF where it reaches 670 nm. This clearly shows that the extra 170 nm bandwidth toward the visible is generated thanks to the decreasing ZDW.

In order to generate even shorter wavelengths, the ZDW-decreasing PCF has been pumped with a more powerful Yb fiber laser delivering 50 W at 1070 nm with a full width at half maximum of 1 nm. With the same setup as described above, we were able to launch a maximum power of 35 W in the fiber, corresponding to a coupling efficiency of 70 %. The resulting experimental spectrum is displayed in Fig. 9. For the highest pump power of 35 W, the SC is ranging from 650 nm to 1380 nm with a 19.5 W output power.

4.3 Discussion and numerical modelling

As claimed above, the basics of using a ZDW decreasing PCF to extend the spectrum towards short wavelengths was to use progressively red-shifted solitons to trap dispersive waves in the visible. The results displayed in Fig. 8 indeed suggest that the long- and short-wavelength edges of the spectra are correlated. In order to have a further insight into the mechanisms of the visible SC formation, the power dynamics of the spectral broadening has been investigated in the ZDW-decreasing PCF for launched powers of 8.2 W, 11.3 W and 13.5 W (see Ref. **?**). As expected, a broadening of the output spectrum occurs on both sides with increasing

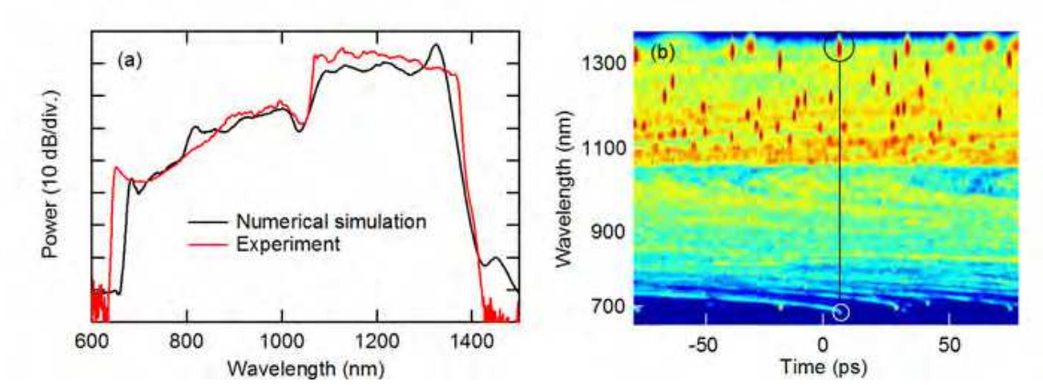

Fig. 9. Experimental (red line) and numerical (black line) output spectra obtained in the ZDW-decreasing PCF for a launched pump power of 35 W. The average power at the fiber output is 19.5 W. Spectrogram of a single-shot simulation at the output of the 200 m-long ZDW-decreasing PCF. The vertical line joins a soliton and its corresponding trapped dispersive wave. The color scale ranges over 30 dB.

launch power inside the fiber. The long and short wavelengths sides were identified by measuring the wavelength of typical spectral features on both edges of the spectrum. The spectral broadening on the long-wavelength side stops at 1140, 1160 and 1250 nm for respective increasing pump powers. The short-wavelength edge is progressively blue-shifted with increasing pump powers and extends to respectively 763, 751 and 720 nm. These experimental results have been compared with the computed group-index curve calculated for the end (small diameter) of the ZDW-decreasing PCF. This is illustrated in Fig. 10, where the group-index curve is plotted as a function of wavelength. Markers represents the long and short wavelength edges experimentally measured for launched powers of 8.2 W (green), 11.3 W (blue) and 13.5 W (red) respectively. The corresponding points for a fixed power are joined by nearly horizontal lines on the plot, which means that these radiations travel at almost the same group velocity when they go out of the fiber. This provides a strong support to the process of group-velocity matching between the most blue- and red-shifted spectral components of each spectrum and this evidences the benefit of the ZDW-decreasing fiber for the generation of shorter wavelengths.

In order to get a deeper understanding of the nonlinear mechanisms originating the visible extension, we performed numerical simulations. We integrated the generalized nonlinear Schrödinger equation including the experimental attenuation curve and all experimental parameters. The numerical method used to model the pump laser was fully described in Ref. Mussot et al. (2007). The simulations were very time consuming (1 week on a standard PC) so we did not perform the usual averaging procedure Mussot et al. (2007) required to account for the experimental measurements. The output spectra resulting from a single simulation is plotted in black line in Fig. 9(a). By performing several other simulations we checked that there was no significant modification from simulation to simulation. The agreement between numerical simulations and experimental results is excellent in terms of shape and extension of the spectrum. It is important to note that numerical simulations have been performed without any free parameters. In both cases, the stop of the spectral broadening at the long-wavelength is due to a relatively high OH absorption around 1380 nm (measured to be about 300 dB/km). The slight discrepancy with experiments observed at short wavelengths (680 nm for the simulations against 650 nm for the experiments) is

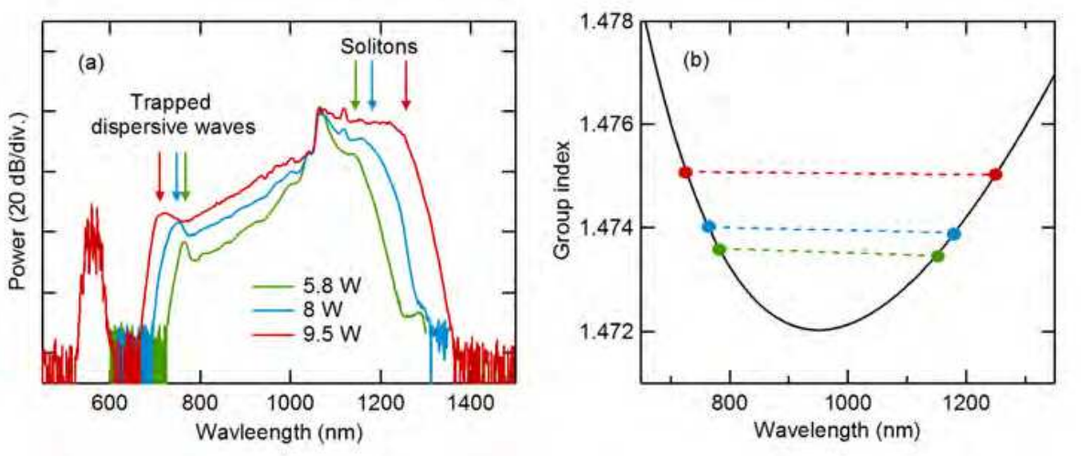

Fig. 10. (a) Output spectra recorded in the ZDW-decreasing PCF for pump powers of 8.2 W (green), 11.3 W (blue) and 13.5 W (red). Output powers are indicated on the graph. (b) Group-index curve calculated at the ZDW-decreasing PCF output (black line). Markers indicate extreme wavelengths of the corresponding SC spectrum experimentally recorded.

probably due to the uncertainty of the calculated GVD curve, leading to a slightly different group-velocity matching condition between red-shifted solitons and trapped dispersive waves. To further illustrate the trapping mechanism responsible for the short wavelength part of the spectrum, the numerical spectrogram of the optical field at the output of the fiber is represented in Fig. 9(b). It corresponds to the numerical spectrum displayed in black line in Fig. 9(a). In the spectrogram, one can see a whole spectral region full of solitons (represented as red dots) originating from the initial MI process. This region extends from the pump wavelength (1070 nm) to the upper limit of the spectrum. Some of the solitons are close to the pump wavelength and some other ones exhibit an important red-shift due to SSFS. The most shifted ones are stopped by the important OH absorption peak at 1380 nm. The region between 680 nm and the pump wavelength corresponds to dispersive waves generated from solitons Travers (2009); Travers et al. (2008). For the most red-shifted solitons, a blue-shifted trapped dispersive wave can be observed just below 700 nm, both travelling at the same group-velocity. An example of a soliton group-velocity matched with a dispersive wave is highlighted in Fig. **??**, where both are joined by a black line. We can see that the trapped dispersive wave is exactly at the vertical of the soliton which confirms that both waves travel at the same velocity inside the fiber. It thus confirms that the extension of the SC towards short wavelengths is mainly due to the trapping of dispersive waves by red-shifted solitons Nishizawa & Goto (2002) rather than by the basic dispersive wave generation process Akhmediev & Karlsson (1995). It should be noted then that the generation of even shorter wavelengths must be possible with the mechanism of dispersive waves trapping by reducing the OH absorption peak, which can be achieved by a careful cleaning treatment during the fiber fabrication process, and/or by enhancing the fiber nonlinearity.

5. White-light continuous-wave supercontinuum

5.1 Benefit of GeO_2 doping

As explained above, CW SC generation is intimately linked to the propagation of fundamental solitons generated from MI. In order to optimize the SC bandwidth, it is thus necessary to

optimize the soliton self-frequency shift effect. One of the most natural solitons to do that is to use GeO_2-doped fibers, because this doping is well known to enhance both Kerr and Raman nonlinearities. However, in order to be usable in CW SC generation experiments, it is important that the ZDW remains slightly lower than the pump wavelength. By adjusting the microstructured cladding properties, it is possible to find some designs with greatly enhance nonlinearity, and still controlled dispersion Barviau et al. (2011). Figure 11 illustrates this. The blue line in (a) correspond to the GVD curve and nonlinear coefficient of a pure silica PCF with a 1060 nm ZDW, and the red line corresponds to a GeO_2-doped PCF with a parabolic profile and a maximum refractive index difference of 20 mol.%. The microstructured cladding parameters have been adjusted so that the doped PCF has the same ZDW of 1060 nm, but in this case, the nonlinear coefficient is enhanced by a factor of about 4 at 1064 nm. Indeed, it reached about 38 $W^{-1}.km^{-1}$ in the GeO_2-doped PCF, against 10 $W^{-1}.km^{-1}$ in the pure silica one. Moreover, Fig. 11(b) shows the enhancement of the material Raman gain due to the presence of GeO_2 as compared to pure silica. A GeO_2-doped PCF corresponding to this design has thus been fabricated, and the pure silica PCF has also been used for comparison.

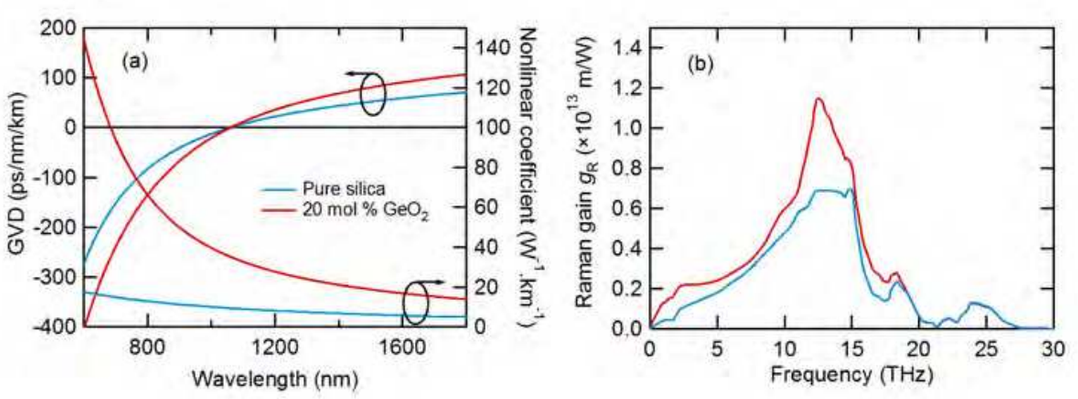

Fig. 11. (a) GVD curves (left axis) and nonlinear coefficient (right axis) calculated for a pure silica PCF (blue) and a PCF doped with a GeO_2 content of 20 mol.%. (b) Raman gain spectra g_R for pure silica (blue) and 20 mol.% GeO_2-doped silica (for a 164 nm pump).

5.2 Spectral extension to the blue

In order to highlight the benefit of using GeO_2-doped PCFs in the context of CW SC generation, both fibers were pumped with a CW fiber laser at 1064 nm in similar conditions. Figure 12(a) shows output spectra obtained for a pump power of 13 W and a length of 300 m for the GeO_2-doped PCF and 400 m for the pure silica one. The SC spectrum looks much broader in the GeO_2-doped PCF than in the pure silica one, yet longer.

As mentioned above, long and short-wavelength SC edges are fixed by a group-velocity matching condition between solitons and trapped dispersive waves Genty et al. (2004; 2005); Gorbach & Skryabin (2007a;b); Gorbach et al. (2006); Travers (2009); Travers & Taylor (2009). Bottom curves in Fig. 12 show group index curves of both fibers, and blue lines illustrates the group-index matching between both SC edges in the pure silica fiber. In the GeO_2-doped one, a dip in the spectral power density appears just below 1380 nm because of soliton accumulation just below the OH absorption band. As a consequence, a dip in the spectral power density can be observed at the corresponding group-velocity matched wavelength (around 805 nm) because of trapped dispersive wave accumulation. From the measurement of

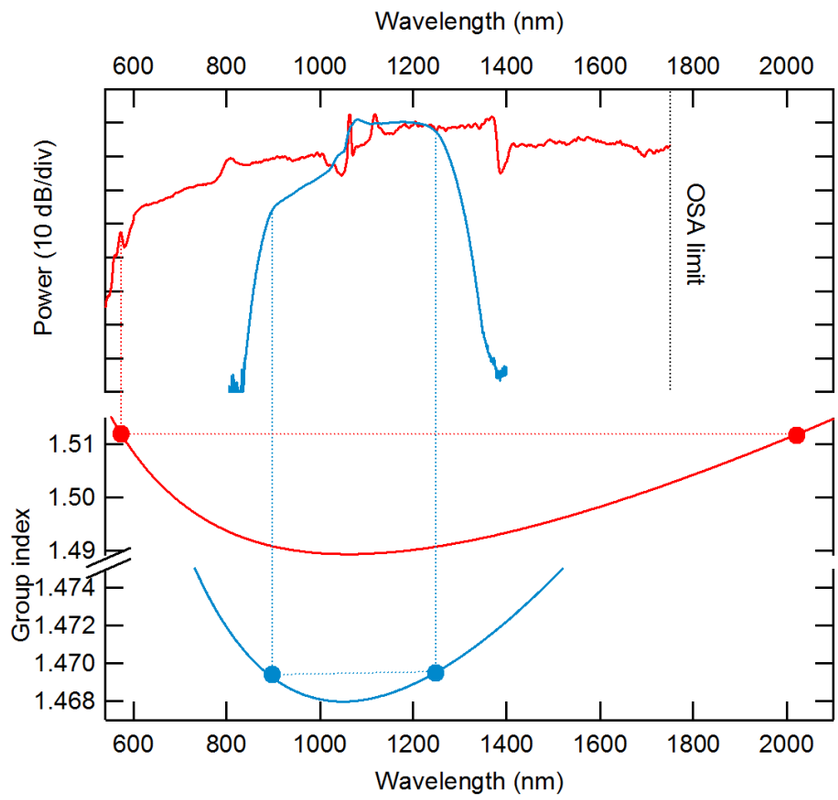

Fig. 12. Top: Supercontinuum generated in the pure silica PCF (blue line) and in the GeO_2-doped one (red line) for a pump power of 13 W. Bottom: corresponding calculated group index curves.

the short wavelength edge (570 nm for the GeO_2-doped PCF) together with the group-index matching, it is thus possible to estimate the long-wavelength one to 2040 nm (not reachable with our optical spectrum analyzer). In this case, there is thus a threefold enhancement of the SC bandwidth (in frequency) as compared to the pure silica PCF.
Note that comparable results in terms of spectral extent have been reported in pure silica PCFs Travers et al. (2008), but with a much higher pump power.

5.3 White-light generation

With the aim of still enhancing the SC bandwidth, it is possible to associate the benefits of GeO_2 doping and fiber tapering presented above. We have thus fabricated a GeO_2-doped ZDW decreasing PCF, characterized by a 50 m long uniform section followed by a 130-m long section over which the outer diameter linearly decreases from 135 to 85 μm. Figure 13(a) shows the spectrum obtained with this fiber for a 45 W pump power. It spans from 470 nm to more than 1750 nm, with an output power of 10 W. A picture of this experiment showing white-light generation is displayed in Fig. 13(b). This is the first demonstration of CW white-light supercontinuum generation.

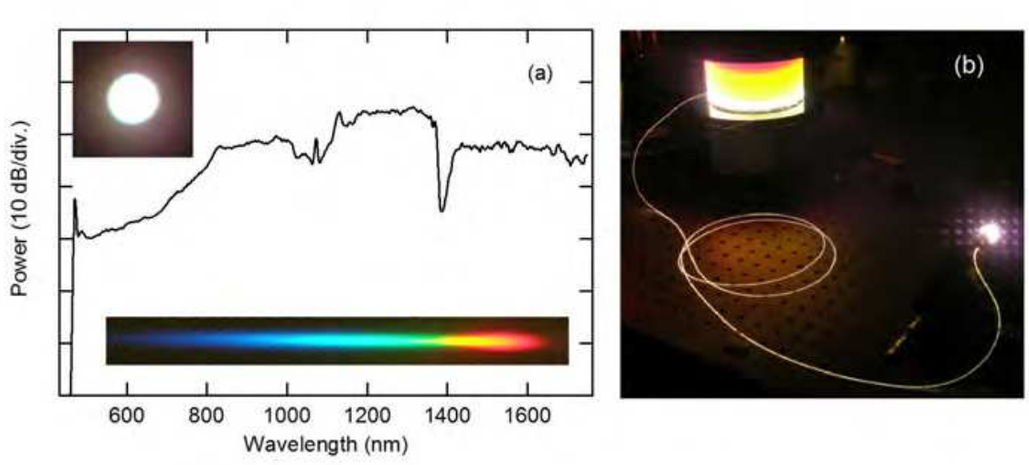

Fig. 13. (a) Supercontinuum generated in a GeO_2-doped ZDW decreasing PCF, with a pump power of 45 W. Top inset: photograph of the output beam far-field. Bottom inset: photograph of the output beam dispersed by a prism. (b) Photograph of the experiment.

6. Conclusion

It is now possible to generate continuous wave supercontinua ranging from the near ultraviolet to the near infrared with spectral power densities in the order of tens of mW/nm. Most of the manipulation of the spectra were carried out by a fine control of the fiber microstructure. These all-fiber sources are very promising for many applications requiring stable and extremely powerful sources.

7. References

Akhmediev, N. & Karlsson, M. (1995). Cherenkov radiation emitted by solitons in optical fibers, *Phys. Rev. A* 51(3): 2602–2607.

Avdokhin, A. V., Popov, S. V. & Taylor, J. R. (2003). Continuous-wave, high-power, Raman continuum generation in holey fibers, *Opt. Lett.* 28(15): 1353–1355.

Barviau, B., Vanvincq, O., Mussot, A., Quiquempois, Y., Melin, G. & Kudlinski, A. (2011). Enhanced soliton self-frequency shift and CW supercontinuum generation in GeO(2)-doped core photonic crystal fibers, *JOURNAL OF THE OPTICAL SOCIETY OF AMERICA B-OPTICAL PHYSICS* 28(5): 1152–1160.

Cumberland, B. A., Travers, J. C., Popov, S. V. & Taylor, J. R. (2008a). 29 W high power CW supercontinuum source, *Opt. Express* 16(8): 5954–5962.

Cumberland, B. A., Travers, J. C., Popov, S. V. & Taylor, J. R. (2008b). Toward visible cw-pumped supercontinua, *Opt. Lett.* 33(18): 2122–2124.

Dudley, J. M., Genty, G. & Coen, S. (2006). Supercontinuum generation in photonic crystal fiber, *Rev. Mod. Phys.* 78(4): 1135–1184.

Efimov, A., Taylor, A., Omenetto, F., Knight, J., Wadsworth, W. & Russell, P. (2003). Phase-matched third harmonic generation in microstructured fibers, *OPTICS EXPRESS* 11(20): 2567–2576.

Genty, G., Lehtonen, M. & Ludvigsen, H. (2004). Effect of cross-phase modulation on supercontinuum generated in microstructured fibers with sub-30 fs pulses, *Opt. Express* 12(19): 4614–4624.

Genty, G., Lehtonen, M. & Ludvigsen, H. (2005). Route to broadband blue-light generation in microstructured fibers, *Opt. Lett.* 30(7): 756–758.

Gonzalez-Herraez, M., Martin-Lopez, S., Corredera, P., Hernanz, M. & Horche, P. (2003). Supercontinuum generation using a continuous-wave Raman fiber laser, *Opt. Commun.* 226(1-6): 323–328.

Gorbach, A. V. & Skryabin, D. V. (2007a). Light trapping in gravity-like potentials and expansion of supercontinuum spectra in photonic-crystal fibres, *Nature Photon.* 1(11): 653–657.

Gorbach, A. V. & Skryabin, D. V. (2007b). Theory of radiation trapping by the accelerating solitons in optical fibers, *Phys. Rev. A* 76(5).

Gorbach, A. V., Skryabin, D. V., Stone, J. M. & Knight, J. C. (2006). Four-wave mixing of solitons with radiation and quasi-nondispersive wave packets at the short-wavelength edge of a supercontinuum, *Opt. Express* 14(21): 9854–9863.

Gordon, J. P. (1986). Theory of the soliton self-frequency shift, *Opt. Lett.* 11(10): 662–664.

Kobtsev, S. & Smirnov, S. (2005). Modelling of high-power supercontinuum generation in highly nonlinear, dispersion shifted fibers at CW pump, *Opt. Express* 13(18): 6912–6918.

Kudlinski, A., George, A., Knight, J., Travers, J., Rulkov, A., Popov, S. & Taylor, J. (2006). Zero-dispersion wavelength decreasing photonic crystal fibers for ultraviolet-extended supercontinuum generation, *Opt. Express* 14(12): 5715–5722.

Kudlinski, A. & Mussot, A. (2008). Visible cw-pumped supercontinuum, *Opt. Lett.* 33(20): 2407–2409.

Mussot, A., Beaugeois, M., Bouazaoui, M. & Sylvestre, T. (2007). Tailoring CW supercontinuum generation in microstructured fibers with two-zero dispersion wavelengths, *Opt. Express* 15(18): 11553–11563.

Nishizawa, N. & Goto, T. (2002). Pulse trapping by ultrashort soliton pulses in optical fibers across zero-dispersion wavelength, *Opt. Lett.* 27(3): 152–154.

Omenetto, F., Taylor, A., Moores, M., Arriaga, J., Knight, J., Wadsworth, W. & Russell, P. (2001). Simultaneous generation of spectrally distinct third harmonics in a photonic crystal fiber, *OPTICS LETTERS* 26(15): 1158–1160.

Persephonis, P., Chernikov, S. & Taylor, J. (1996). Cascaded CW fibre Raman laser source 1.6-1.9 μm, *Electron. Lett.* 32(16): 1486–1487.

Prabhu, M., Kim, N. & Ueda, K. (2000). Ultra-broadband CW supercontinuum generation centered at 1483.4 nm from Brillouin/Raman fiber laser, *Jpn. J. Appl. Phys. Part 2 - Letters* 39(4A): L291–L293.

Skryabin, D., Luan, F., Knight, J. & Russell, P. (2003). Soliton self-frequency shift cancellation in photonic crystal fibers, *Science* 301(5640): 1705–1708.

Stone, J. M. & Knight, J. C. (2008). Visibly "white" light generation in uniform photonic crystal fiber using a microchip laser, *Opt. Express* 16(4): 2670–2675.

Travers, J. C. (2009). Blue solitary waves from infrared continuous wave pumping of optical fibers, *Opt. Express* 17(3): 1502–1507.

Travers, J. C., Rulkov, A. B., Cumberland, B. A., Popov, S. V. & Taylor, J. R. (2008). Visible supercontinuum generation in photonic crystal fibers with a 400W continuous wave fiber laser, *Opt. Express* 16(19): 14435–14447.

Travers, J. C. & Taylor, J. R. (2009). Soliton trapping of dispersive waves in tapered optical fibers, *Opt. Lett.* 34(2): 115–117.

Tse, M., Horak, P., Poletti, F., Broderick, N., Price, J., Hayes, J. & Richardson, D. (2006). Supercontinuum generation at 1.0 mu m in holey fibers with dispersion flattened profiles, *Opt. Express* 14(10): 4445–4451.

Vanholsbeeck, F., Martin-Lopez, S., Gonzalez-Herraez, M. & Coen, S. (2005). The role of pump incoherence in continuous-wave supercontinuum generation, *Opt. Express* 13(17): 6615–6625.

Recent Progress in Optical Fiber Research

Edited by Dr Moh. Yasin

ISBN 978-953-307-823-6

Hard cover, 450 pages

Publisher InTech

Published online 25, January, 2012

Published in print edition January, 2012

This book presents a comprehensive account of the recent progress in optical fiber research. It consists of four sections with 20 chapters covering the topics of nonlinear and polarisation effects in optical fibers, photonic crystal fibers and new applications for optical fibers. Section 1 reviews nonlinear effects in optical fibers in terms of theoretical analysis, experiments and applications. Section 2 presents polarization mode dispersion, chromatic dispersion and polarization dependent losses in optical fibers, fiber birefringence effects and spun fibers. Section 3 and 4 cover the topics of photonic crystal fibers and a new trend of optical fiber applications. Edited by three scientists with wide knowledge and experience in the field of fiber optics and photonics, the book brings together leading academics and practitioners in a comprehensive and incisive treatment of the subject. This is an essential point of reference for researchers working and teaching in optical fiber technologies, and for industrial users who need to be aware of current developments in optical fiber research areas.

InTech Europe

University Campus STeP Ri
Slavka Krautzeka 83/A
51000 Rijeka, Croatia
Phone: +385 (51) 770 447
Fax: +385 (51) 686 166
www.intechopen.com

InTech China

Unit 405, Office Block, Hotel Equatorial Shanghai
No.65, Yan An Road (West), Shanghai, 200040, China
中国上海市延安西路65号上海国际贵都大饭店办公楼405单元
Phone: +86-21-62489820
Fax: +86-21-62489821

IntechOpen